Journal of Genetics and Genomics 47 (2020) 451–465

Contents lists available at ScienceDirect

Journal of Genetics and Genomics

Journal homepage: www.journals.elsevier.com/journal-of-genetics-and-genomics/

Original research

The novel male meiosis recombination regulator coordinates the progression of meiosis prophase I

Miao Li [a, b, *, 1], Haiwei Feng [a, b, 1], Zexiong Lin [a], Jiahuan Zheng [a, b], Dongteng Liu [a, b], Rui Guo [c], Junshi Li [d], Raymond H.W. Li [a, b], Ernest H.Y. Ng [a, b], Michael S.Y. Huen [d], P. Jeremy Wang [c], William S.B. Yeung [a, b], Kui Liu [a, b, *]

[a] Shenzhen Key Laboratory of Fertility Regulation, Center of Assisted Reproduction and Embryology, The University of Hong Kong - Shenzhen Hospital, Shenzhen, 518000, China
[b] Department of Obstetrics and Gynecology, Li Ka Shing Faculty of Medicine, The University of Hong Kong, Hong Kong, 999077, China
[c] Department of Biomedical Sciences, University of Pennsylvania School of Veterinary Medicine, Philadelphia, PA, 19104, USA
[d] School of Biomedical Sciences, Li Ka Shing Faculty of Medicine, The University of Hong Kong, Hong Kong, 999077, China

ARTICLE INFO

Article history:
Received 26 July 2020
Received in revised form
20 August 2020
Accepted 21 August 2020
Available online 26 August 2020

Keywords:
Meiosis
4930432K21Rik
Recombination
Ubiquitination

ABSTRACT

Meiosis is a specialized cell division for producing haploid gametes in sexually reproducing organisms. In this study, we have independently identified a novel meiosis protein male meiosis recombination regulator (MAMERR)/4930432K21Rik and showed that it is indispensable for meiosis prophase I progression in male mice. Using super-resolution structured illumination microscopy, we found that MAMERR functions at the same double-strand breaks as the replication protein A and meiosis-specific with OB domains/spermatogenesis associated 22 complex. We generated a *Mamerr*-deficient mouse model by deleting exons 3–6 and found that most of *Mamerr*$^{-/-}$ spermatocytes were arrested at pachynema and failed to progress to diplonema, although they exhibited almost intact synapsis and progression to the pachytene stage along with XY body formation. Further mechanistic studies revealed that the recruitment of DMC1/RAD51 and heat shock factor 2–binding protein in *Mamerr*$^{-/-}$ spermatocytes was only mildly impaired with a partial reduction in double-strand break repair, whereas a substantial reduction in ubiquitination on the autosomal axes and on the XY body appeared as a major phenotype in *Mamerr*$^{-/-}$ spermatocytes. We propose that MAMERR may participate in meiotic prophase I progression by regulating the ubiquitination of key meiotic proteins on autosomes and XY chromosomes, and in the absence of MAMERR, the repressed ubiquitination of key meiotic proteins leads to pachytene arrest and cell death.

1. Introduction

As a specialized type of cell division in sexually reproducing eukaryotes, meiosis creates haploid germ cells from diploid progenitors and guarantees their genetic diversity (Zickler and Kleckner, 1999; Handel and Schimenti, 2010). Meiosis prophase I starts with the programmed formation of DNA double-strand breaks (DSBs) generated by the topoisomerase-like protein SPO11, and the DSBs are then resected to produce 3′ single-stranded DNA overhangs and subsequently repaired through homologous recombination (HR) involving homologous pairing and strand exchange (Keeney and Neale, 2006; Baudat et al., 2010).

Multiple proteins take part in HR and drive the maturation of crossovers or noncrossovers. The replication protein A (RPA) complex (RPA1, RPA2, and RPA3) directly coats single-stranded DNA to protect it from degradation and to remove secondary structures (Wold, 1997; Ribeiro et al., 2016). The presence of RAD51 and DMC1 on presynaptic filaments is essential for proper strand invasion (Cloud et al., 2012), but the processes behind the formation and stabilization of the RAD51/DMC1 nucleofilament are still not completely understood. Recent studies have suggested that heat shock factor 2–binding protein (HSF2BP) might facilitate the recruitment of breast cancer susceptibility gene 2 (BRCA2), which in turn mediates the localization of recombinases

* Corresponding authors.
E-mail addresses: miaoli@hku.hk (M. Li), kliugc@hku.hk (K. Liu).
[1] These authors contributed equally to this work.

https://doi.org/10.1016/j.jgg.2020.08.001

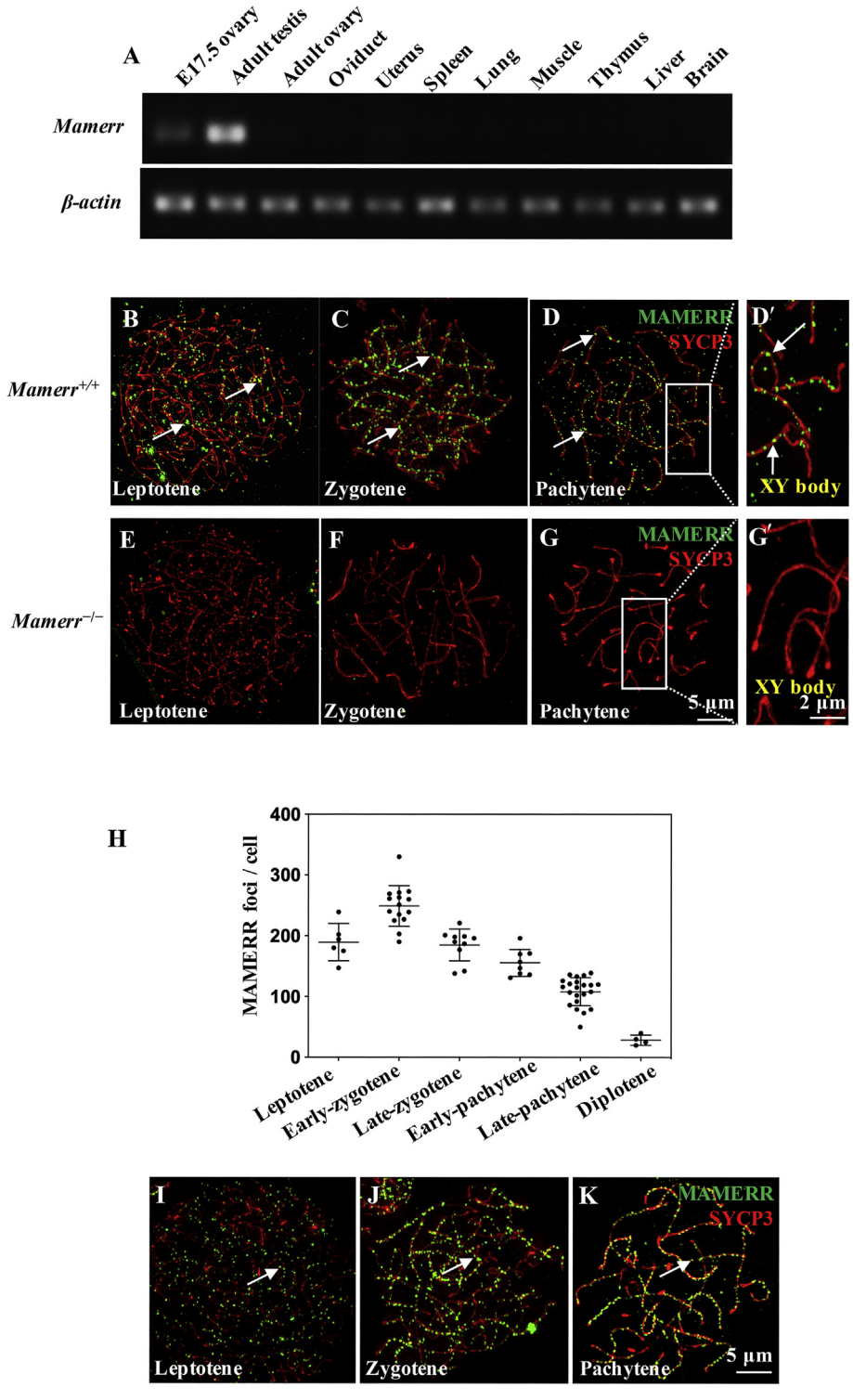

Fig. 1. Expression and localization of MAMERR during meiosis prophase I. **A**: Reverse transcription polymerase chain reaction (RT-PCR) detection of *Mamerr* in different tissues indicated that *Mamerr* was specifically expressed in adult testes and E17.5 ovaries. β-actin was used as the internal control. **B**–**D**: SIM images of MAMERR localization on meiotic chromosomes in *Mamerr*$^{+/+}$ and *Mamerr*$^{-/-}$ spermatocytes. MAMERR (green signal) was located on the SYCP3 (red signal)-marked autosome and chromosome axes (arrows). The enlarged view of the boxed area shows that MAMERR was localized on the X and Y chromosomes (**D′**, arrows). **E**–**G**: In *Mamerr*$^{-/-}$ spermatocytes, no MAMERR signal on chromosomes was detected. The enlarged view of the boxed chromosomes shows that no MAMERR was detected on the X and Y chromosomes (**G′**). **H**: The numbers of MAMERR foci at each meiotic stage. **I**–**K**: Chromosome spreads of oocytes from E17.5 *Mamerr*$^{+/+}$ and *Mamerr*$^{-/-}$ ovaries were stained for MAMERR (green) and SYCP3 (red). MAMERR was located on the chromosome axis from the leptotene to pachytene stages (arrows). MAMERR, male meiosis recombination regulator; SIM, structured illumination microscopy; SYCP3, synaptonemal complex protein 3.

RAD51 and DMC1 at the meiotic DSBs (Brandsma et al., 2019). This notion was based on the finding that deletion of *Hsf2bp* led to the failure of synapsis and abolished the localization of RAD51/DMC1 (Brandsma et al., 2019). The presynaptic filament searches for its homologous sequence and invades the homologous chromosome, leading to a structure known as a displacement loop (Zickler and Kleckner, 2015). At this phase, meiosis-specific with OB domains (MEIOB) and its cofactor spermatogenesis associated 22 (SPATA22) mediate second-end capture (Luo et al., 2013). The DSBs are then processed to form crossovers or noncrossovers (Baker et al., 1996). The prominent features at the pachytene stage of prophase I include the partial synapsis of the X and Y chromosomes at their pseudoautosomal regions (PARs), the formation of the XY body, and meiotic sex chromosome inactivation (MSCI) (Turner, 2007).

MEIOB and SPATA22 form an obligate complex during meiosis (Luo et al., 2013; Hays et al., 2017), and the MEIOB/SPATA22 and the RPA complexes colocalize on chromosomes during meiosis and interact with each other (Xu et al., 2017). A recent study has shown that HSF2BP also colocalizes with RPA and MEIOB/SPATA22 complexes to facilitate RAD51/DMC1 recruitment (Brandsma et al., 2019). These proteins are essential for HR and DSB repair, and mice lacking these proteins present with meiosis arrest at the zygotene stage with failed synapsis and DSB repair. However, the mechanism how these recombination-related proteins appear, degrade, and collaborate with each other so that the meiosis progression occurs properly remains poorly understood.

A recent study showed that ubiquitin is localized on the chromosome axis and regulates the stabilization and degradation of recombination factors to enable the proper occurrence of synapsis, DSB repair, and crossover formation (Rao et al., 2017). In addition, the ubiquitin-proteasome system coordinates with small ubiquitin-like modifier modification to regulate cellular proteostasis (Reynolds et al., 2013; Qiao et al., 2014; Rao et al., 2017). In mice lacking the polyubiquitin gene ubiquitin B (*Ubb*), spermatocytes exhibited decreased ubiquitination and were arrested at the pachytene stage (Ryu et al., 2008; Sinnar et al., 2011). Moreover, the germ line–specific protein Scm polycomb group protein like 2 (SCML2) has been reported to mediate the repression of genes by differentially regulating histone H2A ubiquitination on autosomes and sex chromosomes during meiosis and thereby regulating the germ line epigenome and male reproduction (Hasegawa et al., 2015; Luo et al., 2015).

Here, we have independently identified a novel male germ cell–specific protein in mice, male meiosis recombination regulator (MAMERR), that regulates the recruitment of the meiotic recombinases RAD51 and DMC1 and promotes the ubiquitination of the autosomes and XY body. Male *Mamerr*$^{-/-}$ mice were sterile, and the DMC1/RAD51 recruitment in *Mamerr*$^{-/-}$ spermatocytes was partially compromised, leading to some unrepaired meiotic DSBs on autosomes. More importantly, *Mamerr*$^{-/-}$ spermatocytes showed substantially reduced ubiquitination on the autosomes and XY body, accompanied by pachytene arrest and germ cell death. In contrast, female *Mamerr*$^{-/-}$ mice were fertile. We propose that MAMERR plays an indispensable role in guiding the progression of meiosis prophase I by regulating the ubiquitination status of sex chromosomes and autosomes.

2. Results

2.1. MAMERR is a meiosis prophase I–specific protein in mouse germ cells

We isolated and purified different types of male germ cells using bovine serum albumin gradient sedimentation (Gan et al., 2013). We performed mRNA sequencing of spermatogonia, leptotene/zygotene spermatocytes, pachytene spermatocytes, round sperms, the spleen, the kidney, and the liver, and we independently found the gene coded by *4930432K21Rik*, which we named *Mamerr*. *Mamerr* was highly expressed in spermatocytes from leptotene/zygotene and pachytene stages to round spermatids, but was expressed at very low levels in spermatogonia and somatic organs (Fig. S1A). This gene was initially published as one of the 104 meiosis prophase I–specific genes in mouse female germ cells by David Page's laboratory (see Table S2 in the study by Soh et al., 2015). Meanwhile, it was also identified as a testis-specific gene through RNA sequencing in Professor Yoshinori Watanabe's laboratory of the University of Tokyo, Japan (personal communication). Reverse transcription polymerase chain reaction (RT-PCR) analysis confirmed that *Mamerr* was specifically expressed in germ line tissues, including adult testes and embryonic ovaries (Fig. 1A). Amino acid sequence alignment showed that MAMERR is conserved in mice, rats, and humans (Fig. S1B).

2.2. MAMERR protein was expressed as foci on the axes of autosomes and sex chromosomes during meiosis prophase I

We performed immunofluorescence staining of MAMERR in spread spermatocyte nuclei and detected the precise chromosomal localization of MAMERR using super-resolution structured illumination microscopy (SIM). The MAMERR signal was found to be localized on synaptonemal complex protein 3 (SYCP3)–stained chromosome axes during meiosis prophase I (Fig. 1B–D, arrows). MAMERR foci were also observed on XY chromosomes (Fig. 1D', arrows). As a negative control, no MAMERR expression was seen in *Mamerr*$^{-/-}$ spermatocytes (Fig. 1E–G, G', see the following section for the generation of *Mamerr*$^{-/-}$ mice). The expression pattern of MAMERR in meiotic chromosomes was very similar to other recombinase-related proteins such as RPA2 (Shi et al., 2019), MEIOB (Luo et al., 2013), and SPATA22 (La Salle et al., 2012).

At the leptotene stage, there was a mean of 189 MAMERR foci per cell, and the number of foci reached a peak at the early zygotene stage, with a mean of 250 foci per spermatocyte (Fig. 1H). The number of MAMERR foci began to decrease at the late zygotene (185 foci/cell) and early pachytene (155 foci/cell) stages. It is worth noting that MAMERR expression persisted on chromosomes at the late pachytene stage (Fig. 1H), which is in contrast to RPA2 that is already absent by this stage (Shi et al., 2019). We also performed chromosome spreading with embryonic day 17.5 (E17.5) ovaries and found a similar pattern of MAMERR localization on chromosome axes of meiotic female germ cells (Fig. 1I–K, arrows).

2.3. MAMERR foci colocalized with RPA-MEIOB/SPATA22 complexes and HSF2BP

To clarify whether the MAMERR localization is DSB dependent, we first stained for MAMERR in *Spo11*$^{+/+}$ and *Spo11*$^{-/-}$ spermatocytes. We found that compared with *Spo11*$^{+/+}$ spermatocytes where MAMERR foci were localized on the chromosome axis (Fig. 2A, arrows), the MAMERR foci were abolished in *Spo11*$^{-/-}$ spermatocytes (Fig. 2B). These results suggest that MAMERR recruitment only occurs after the formation of DSBs. Considering the similar expression patterns of MAMERR and RPA2, we performed the MAMERR and RPA2 colocalization experiment and found that MAMERR foci largely overlapped with RPA2 foci at the zygotene stage as observed under SIM (Fig. 2C, D and D', arrows). We then studied the colocalization of MAMERR with other meiosis and recombinase-related proteins and found that MAMERR colocalized with SPATA22 (Fig. 2E, F and F', arrows) and HSF2BP (Fig. 2G, H and H', arrows), but did not colocalize with DMC1 foci (Fig. 2I, J and J').

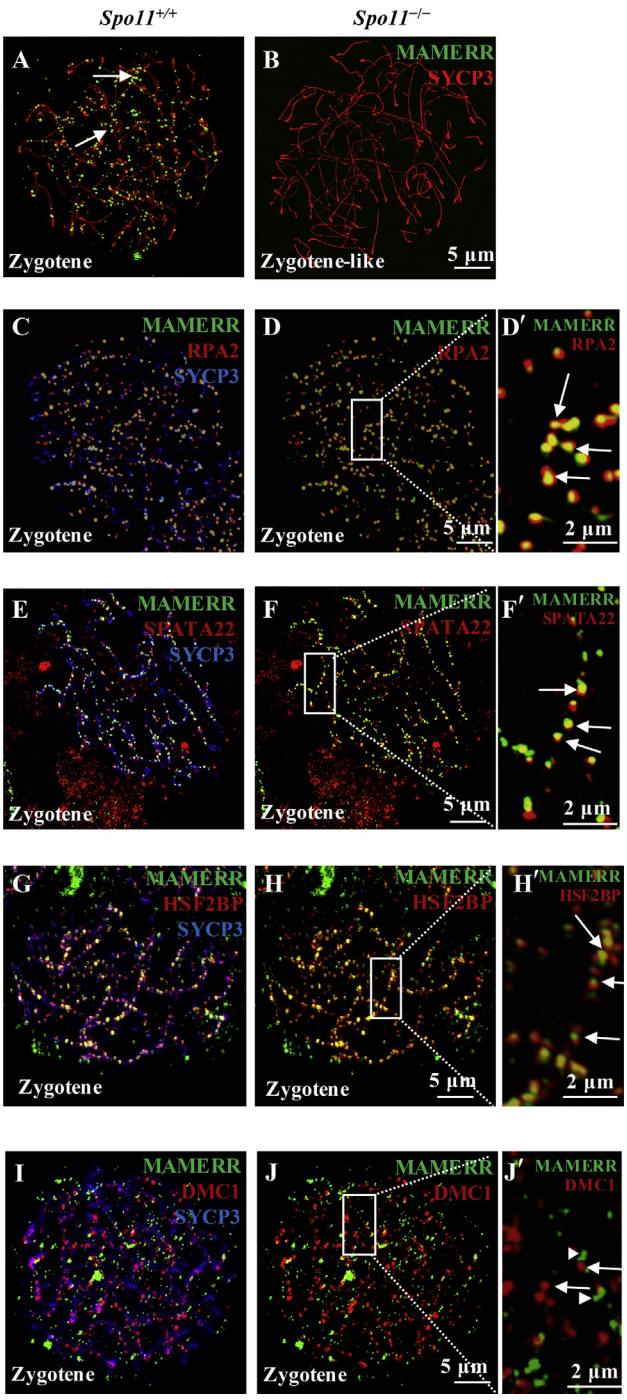

Fig. 2. MAMERR colocalized with RPA/MEIOB/SPATA22 complexes and HSF2BP. **A** and **B**: SIM images of MAMERR and SYCP3 immunostaining of chromosome spreads from *Spo11*$^{+/+}$ and *Spo11*$^{-/-}$ spermatocytes. MAMERR foci were absent in *Spo11*$^{-/-}$ zygotene-like spermatocytes. **C** and **D**: Colocalization of MAMERR (green) and RPA2 (red) in zygotene spermatocytes. The enlarged view of the boxed area shows MAMERR colocalized with RPA2 (**D′**, arrows). **E** and **F**: Colocalization of MAMERR (green) and SPATA22 (red) in zygotene spermatocytes. The enlarged view of the boxed area shows that MAMERR colocalized with SPATA22 (**F′**, arrows). **G** and **H**: Colocalization of MAMERR (green) and HSF2BP (red) in zygotene spermatocytes. The enlarged view shows MAMERR colocalized with HSF2BP (**H′**, arrows). **I** and **J**: Colocalization of MAMERR (green) and DMC1 (red) in zygotene spermatocytes. The enlarged view of the boxed area shows that MAMERR did not colocalize with DMC1 (**J′**). Arrows indicate DMC1 foci, and arrowheads indicate MAMERR foci. MAMERR, male meiosis recombination regulator; SIM, structured illumination microscopy; SYCP3, synaptonemal complex protein 3; RPA, replication protein A; MEIOB, meiosis-specific with OB domains; SPATA22, spermatogenesis associated 22; HSF2BP, heat shock factor 2–binding protein.

2.4. Deletion of Mamerr disrupted meiosis progression with most male germ cells arrested at the pachytene stage

To study the functional roles of MAMERR, we generated a *Mamerr*-deficient mouse model. The *Mamerr* gene is composed of nine exons, with an *ATG* start codon in exon 2 and a *TAA* stop codon in exon 9. The *Mamerr*-knockout mouse model carried a deletion of the genomic DNA fragment covering exon 3 to exon 6 (Fig. S2A). Western blot analysis confirmed the absence of MAMERR protein in *Mamerr*$^{-/-}$ testes (Fig. 3A).

Mamerr$^{-/-}$ males were found to be sterile with a reduced testis size (Fig. 3B). Histological analysis showed that postnatal day 35 *Mamerr*$^{+/+}$ testes contained differentiated spermatocytes at various stages and elongated spermatids (Fig. 3C, arrows), while *Mamerr*$^{-/-}$ testes lacked postmeiotic spermatids (Fig. 3D, arrow), and spermatocyte nuclei with condensed chromatin were observed (Fig. 3D, arrowhead). In contrast to males, the fertility of *Mamerr*$^{-/-}$ females was normal.

To determine the cause of the meiotic defects in *Mamerr*$^{-/-}$ mice, we performed chromosome spreading and analyzed the progression of meiosis prophase I in *Mamerr*$^{-/-}$ male germ cells by staining for synaptonemal complex protein 1 (SYCP1) and SYCP3. To look into the chromosomal structure and stability of the synaptonemal complex in *Mamerr*$^{-/-}$ spermatocytes in greater detail, we stained for the N-terminus of SYCP1. We found that in *Mamerr*$^{-/-}$ spermatocytes, SYCP1–N was localized in the midline of the synaptonemal complex in both *Mamerr*$^{+/+}$ (Fig. S2B–D and B'–D', arrows) and *Mamerr*$^{-/-}$ mice (Fig. S2E–G and E'–G', arrowheads). Similar to *Mamerr*$^{+/+}$ spermatocytes, in *Mamerr*$^{-/-}$ pachytene spermatocytes, the autosomes achieved full synapsis as indicated by the SYCP1 signal (Fig. S2F and F', arrowheads). This is supported by a concurrent study in which a subpopulation of *Mamerr* (*Brme1*)-knockout spermatocytes 'indeed showed a pachytene morphology, whose 19 pairs of autosomal axes were apparently fully synapsed' in a knockout mouse model wherein a complete deletion of exons 3–9 of the *Mamerr/4930432K21rik* gene was performed (Takemoto et al., 2020). The morphologically normal synapsis in *Mamerr*$^{-/-}$ spermatocytes in this study and in the study by Takemoto et al., 2020 was different from that seen in another study using a partial knockout mouse model wherein exon 7 and part of exon 8 of *Mamerr* were deleted (Zhang et al., 2020). This incomplete knockout strategy might affect the phenotypes because a partial MAMERR protein encoded by intact exons 1–6 of the *Mamerr* gene may still exist (Zhang et al., 2020).

We also observed that similar to *Mamerr*$^{+/+}$ cells (Fig. S2C), the sex chromosomes in *Mamerr*$^{-/-}$ pachytene cells were partially synapsed in the PAR (Fig. S2F, white-dashed circle). Thus, the observed *Mamerr*$^{-/-}$ spermatocytes had progressed to the pachytene stage. We quantified the number of spermatocytes at different prophase stages using testes from 8-week-old mice. In *Mamerr*$^{+/+}$ mice, cells at the pachytene stage represented 55% of the total cell counts, and 29% of the cells had entered the diplotene stage (Fig. 3E). In contrast, in *Mamerr*$^{-/-}$ mice, there was a higher proportion of pachytene spermatocytes (68%) (Fig. 3E, arrow), whereas the proportion of diplotene cells was low (4%) (Fig. 3E). No metaphase I spermatocytes were seen in *Mamerr*$^{-/-}$ mice. These results show that progression of meiosis prophase I from leptotene to diplotene stages in *Mamerr*$^{-/-}$ mice was slower, with most of the germ cells being arrested at the pachytene stage (Fig. 3E, arrow).

2.5. DSB repair and crossover formation are mildly defective in Mamerr$^{-/-}$ *mice*

Considering the seemingly normal synapsis but pachytene arrest in *Mamerr*$^{-/-}$ spermatocytes, we analyzed DSB repair and crossover

formation in *Mamerr*$^{-/-}$ spermatocytes. In *Mamerr*$^{-/-}$ zygotene spermatocytes, γH2AX signals were observed at a comparable intensity as in *Mamerr*$^{+/+}$ spermatocytes (Fig. 3F and I). In *Mamerr*$^{+/+}$ pachytene and diplotene stages, the γH2AX signal was restricted to sex chromosomes (Fig. 3G and H, white-dashed circles). However, in *Mamerr*$^{-/-}$ spermatocytes at the pachytene and diplotene stage, in addition to the strong γH2AX signals on the XY body (Fig. 3J and K, white-dashed circles), γH2AX remained as specific foci scattered across the autosomes, as shown by SIM (Fig. 3J, J' and K, yellow arrows). We then immunostained for MutL homolog 1 (MLH1) to identify crossover maturation in the pachytene stage (Edelmann et al., 1996). We found normal MLH1 foci in *Mamerr*$^{+/+}$ pachytene spermatocytes (Fig. 3L, arrows, and N), but this was reduced to a mean of 10 MLH1 foci in pachytene *Mamerr*$^{-/-}$ spermatocytes (Fig. 3M, arrowheads, and N). These results show that DSBs were produced normally in *Mamerr*$^{-/-}$ spermatocytes but were only partially repaired, with compromised crossover maturation.

2.6. Localization of MAMERR foci on chromosomes is dependent on the RPA-MEIOB/SPATA22 complex, but not vice versa

To determine the functional relationships between MAMERR and other known DSB-associated meiotic proteins, including RPAs, SPATA22, RAD51, and DMC1, we detected the presence and localization of these proteins in *Mamerr*$^{-/-}$ spermatocytes. We found that at the zygotene stage, the numbers of RPA2 foci were similar between *Mamerr*$^{+/+}$ (Fig. 4A, arrows) and *Mamerr*$^{-/-}$ (Fig. 4B, arrows) spermatocytes (Fig. 4G, zygotene). In *Mamerr*$^{-/-}$ pachytene spermatocytes, there were more RPA2 foci (Fig. 4D, arrows) than *Mamerr*$^{+/+}$ spermatocytes (Fig. 4C, arrows). At the diplotene stage, RPA2 foci had disappeared in *Mamerr*$^{+/+}$ cells (Fig. 4E), whereas RPA2 foci were still detected in *Mamerr*$^{-/-}$ cells (Fig. 4F, arrows). We found a mean of 15 persistent RPA2 foci on each chromosome (Fig. 4G, diplotene). In *Mamerr*$^{-/-}$ spermatocytes, the numbers of SPATA22 foci were comparable with *Mamerr*$^{+/+}$ spermatocytes during the zygotene to pachytene stage (Fig. S3A-E, arrows). These results showed that the formation and loading of the RPA2 and MEIOB/SPATA22 complex on DSBs are independent of MAMERR. It is likely that MAMERR only plays a regulatory role in prophase I rather than being an indispensable component for forming the RPA2 and MEIOB/SPATA22 complex.

To determine whether MAMERR localization was dependent on the RPA2 and MEIOB/SPATA22 complex, we next stained for MAMERR in *Rpa1* conditional knockout mice (referred to as *Rpa1*^{cKO} mice). Defective zygotene-like spermatocytes were present in *Rpa1*^{cKO} testes as indicated by a lack of synapsis and unusually strong γH2AX signals (Fig. 4I, blue signal) as we previously reported (Shi et al., 2019). We found that in contrast to the abundant MAMERR expression in wild-type cells (Fig. 4H, arrows), in *Rpa1*^{cKO} zygotene-like spermatocytes, MAMERR foci were completely absent on chromosomes (Fig. 4I). We then analyzed MAMERR expression in *Meiob*$^{+/+}$ (Fig. 4J, arrows) and *Meiob*$^{-/-}$ spermatocytes (Luo et al., 2013) and found that MAMERR foci were also completely absent in *Meiob*$^{-/-}$ spermatocytes (Fig. 4K). Thus, the localization of MAMERR foci on chromosomes is dependent on the RPA and MEIOB/SPATA22 complex, but RPA2 and SPATA22 localization is independent on MAMERR.

2.7. Deletion of Mamerr partially impairs recruitment of DMC1 and RAD51

As meiosis progresses, the recruited meiotic recombinases DMC1 and RAD51 displace RPA and promote the search for a homologous chromosome. We found that DMC1 and RAD51 recruitment in *Mamerr*$^{-/-}$ spermatocytes was partially defective. As shown in Fig. 5E, there was a significant reduction in DMC1 recruitment in *Mamerr*$^{-/-}$ spermatocytes from the zygotene to pachytene stages (Fig. 5C and D) compared with *Mamerr*$^{+/+}$ spermatocytes (Fig. 5A and B). It is worth noting, however, that the recruitment of DMC1 in *Mamerr*$^{-/-}$ spermatocytes was not completely abolished (Fig. 5E). In *Mamerr*$^{-/-}$ spermatocytes at the zygotene and pachytene stages, there were still a mean of 60 and 20 DMC1 foci, respectively (Fig. 5E). Moreover, compared with *Mamerr*$^{+/+}$ spermatocytes (Fig. 5F and G), the number of RAD51 foci in *Mamerr*$^{-/-}$ spermatocytes decreased at the zygotene and pachytene stages (Fig. 5H and I). RAD51 was, however, still found to be recruited to chromosomes, with an average of 92 foci at the zygotene stage and 34 foci at the pachytene stage (Fig. 5J).

It was apparent that the DMC1/RAD51 complexes were still recruited to *Mamerr*$^{-/-}$ chromosomes, indicating that the recombinase recruitment in mutant spermatocytes was only mildly disturbed. In the absence of MAMERR, DMC1/RAD51 could still be partially recruited, implying that MAMERR might play a facilitating role rather than a direct recruiting function for DMC1 and RAD51.

2.8. MAMERR localization is fully dependent on HSF2BP, and HSF2BP recruitment is partially disrupted in Mamerr$^{-/-}$ spermatocytes

HSF2BP was reported to bind to BRCA2 and was hypothesized to recruit BRCA2 to DSBs (Brandsma et al., 2019), where BRCA2 recruits RAD51 and DMC1 (Thorslund et al., 2007; Jensen et al., 2010). The colocalization experiment by high-resolution SIM has shown that MAMERR signals overlapped with HSF2BP foci (Fig. 2G, H and H', arrows). We next detected MAMERR expression in *Hsf2bp*$^{-/-}$ cells and found that compared with the MAMERR foci observed in *Hsf2bp*$^{+/+}$ spermatocytes (Fig. 5K, arrows), MAMERR foci at DSBs in *Hsf2bp*$^{-/-}$ spermatocytes were completely abolished (Fig. 5L). This shows that MAMERR localization on DSBs is fully dependent on HSF2BP. We next found that compared with the numbers of HSF2BP foci in *Mamerr*$^{+/+}$ germ cells (Fig. 5M, N and Q), the number of HSF2BP foci decreased by 40% and 38% in *Mamerr*$^{-/-}$ zygotene and pachytene spermatocytes, respectively (Fig. 5O–Q). These results suggest that the localization of MAMERR on DSBs is dependent on HSF2BP, whereas the localization of HSF2BP on DSBs is not fully dependent on MAMERR. It is thus likely that MAMERR modifies HSF2BP and regulates the function of HSF2BP in the context of RAD51/DMC1 recruitment.

2.9. MAMERR is found in the same protein complex with HSF2BP and RPA2 in vitro

Based on the aforementioned results, we hypothesized that MAMERR and HSF2BP exist in the same functional protein complex. We tested this hypothesis in HEK 293T cells, where no endogenous MAMERR was expressed. HEK 293T cells were cotransfected with *pCAG-Gfp-Mamerr* and *pcDNA3.1-Hsf2bp-His* constructs. By performing immunoprecipitation (IP) with a green fluorescent protein (GFP) antibody, we found that HSF2BP-His coprecipitated with GFP-MAMERR (Fig. S4B). These results supported our hypothesis that MAMERR and HSF2BP occur in the same protein complex and that there are interactions between them.

To identify the amino acid (aa) regions that are essential for associating MAMERR in the same complex with HSF2BP, we constructed a series of truncated *Gfp-Mamerr* constructs (Fig. S4A). Starting by splitting the protein into two fragments (MAMERR 1–300 aa and MAMERR 301–600 aa) and four fragments (MAMERR 1–150 aa, 151–300 aa, 301–450 aa, and 451–600 aa), we found that the MAMERR 301–600 aa (Fig. S4D) and 451–600 aa regions (Fig. S4H) could be immunoprecipitated with HSF2BP in HEK

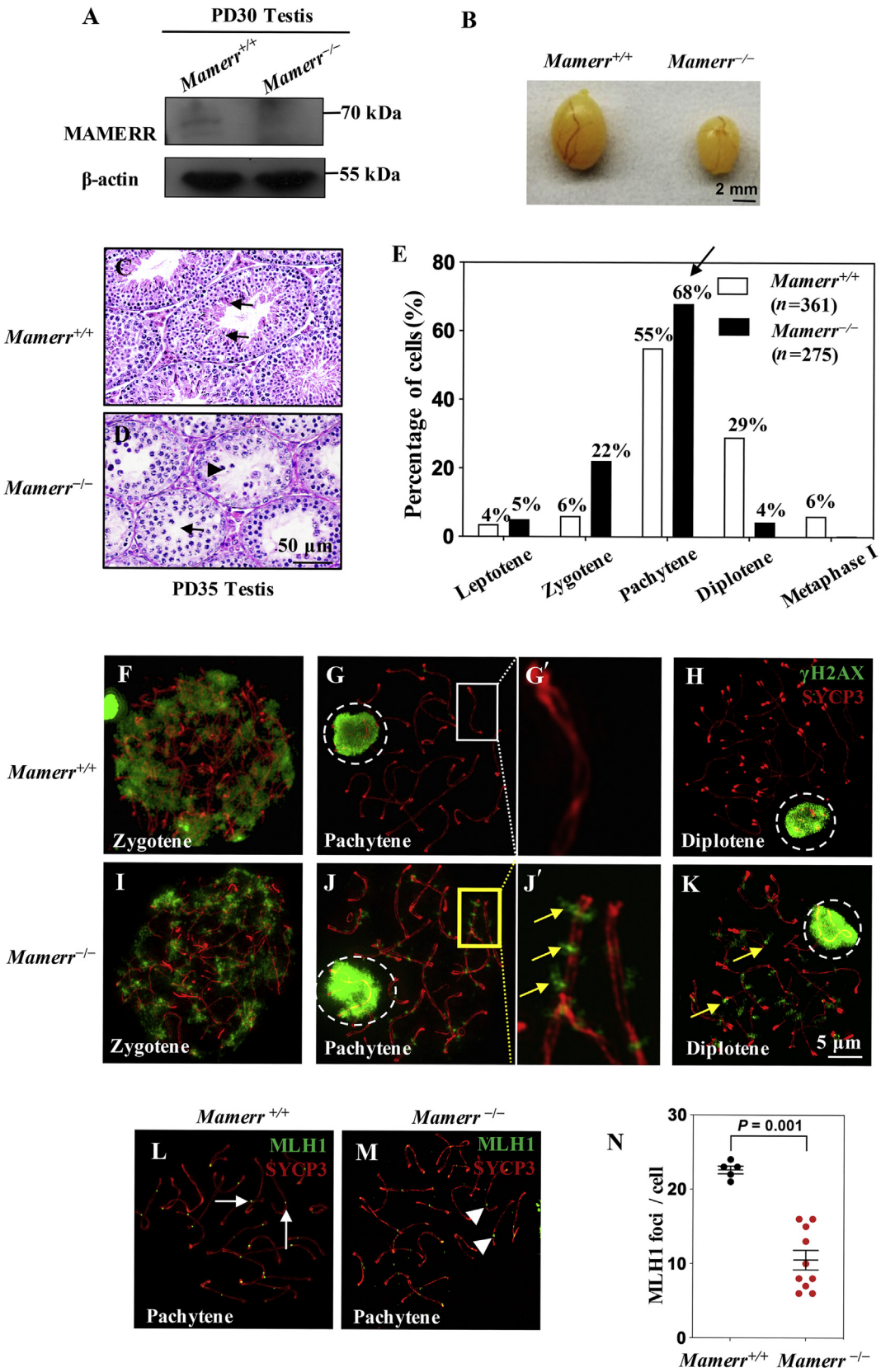

Fig. 3. MAMERR is indispensable for maintaining male fertility. **A**: Western blotting showed that MAMERR was deleted in PD30 *Mamerr*$^{-/-}$ testes compared with *Mamerr*$^{+/+}$ testes. β-actin was used as the loading control. **B**: *Mamerr*$^{-/-}$ male mice had a reduced testis size at PD35 compared with *Mamerr*$^{+/+}$ mice. **C** and **D**: Hematoxylin and eosin staining of sections of adult *Mamerr*$^{+/+}$ and *Mamerr*$^{-/-}$ testes showed a complete arrest of spermatogenesis. Arrowheads show the condensed nuclei, and the arrow shows the seminiferous tubule's lack of postmeiotic spermatocytes. **E**: Percentages of spermatocytes at different stages of meiosis prophase I in 8-week-old *Mamerr*$^{+/+}$ and *Mamerr*$^{-/-}$ testes. The numbers marked above the bars show the percentages of cells at the indicated meiosis stage. **F**–**K**: Chromosome spreads of spermatocytes from *Mamerr*$^{+/+}$ and *Mamerr*$^{-/-}$ males were stained with SYCP3 (red) and γH2AX (green). (**F** and **I**). Representative images of spermatocytes at the zygotene stage are shown. **G** and **J**: Representative images of spermatocytes at

293 cells, as indicated by the green lines in Fig. S4A. To further locate the interacting domain of MAMERR, we shortened the MAMERR 451–600 aa construct further into six truncated constructs (Fig. S4A). MAMERR 451–575 aa (Fig. S4K), 476–600 aa (Fig. S4L), 501–600 aa (Fig. S4M), and 526–600 aa (Fig. S4N) could immunoprecipitate with HSF2BP (Fig. S4A, green lines), whereas MAMERR 451–525 aa (Fig. S4I) and 451–550 aa (Fig. S4J) showed no coprecipitation with HSF2BP (Fig. S4A, red lines). Thus, we concluded that the 50-aa region (526–575 aa) in MAMERR is responsible for interacting with or forming the protein complex with HSF2BP (Fig. S4A, arrow).

Because we found that RPA2 remained on chromosomes at the diplotene stage in *Mamerr*$^{-/-}$ spermatocytes, we speculated that MAMERR may interact with the RPA complex. HEK 293T cells were cotransfected with mouse *pCAG-Gfp-Mamerr* and *pcDNA3.1-Rpa2-Flag* constructs. By performing IP with a GFP antibody, we found that RPA2-FLAG protein was coprecipitated with GFP-MAMERR (Fig. S5A), suggesting that MAMERR interacts with RPA2.

2.10. The *Mamerr*$^{-/-}$ XY body shows substantially suppressed ubiquitination

Mamerr$^{-/-}$ spermatocytes progressed to the pachytene stage with successful formation of the XY body (Fig. S2F, white-dashed circle). Considering the persistent expression of MAMERR on sex chromosomes and the pachytene arrest phenotype in *Mamerr*$^{-/-}$ spermatocytes, we hypothesized that MAMERR plays a role in the pachytene XY body in addition to its regulating/modifying role in mediating DMC1/RAD51 recruitment at the zygotene stage.

To this end, we tested whether ubiquitin modification of sex chromosomes was altered in *Mamerr*$^{-/-}$ male germ cells. We first used an antibody clone FK2 that recognizes mono and lysine (K)-29-, K-48-, and K-63-linked polyubiquitinylated conjugates (Lu et al., 2010). Similar to previous studies (Ichijima et al., 2011; Lu et al., 2013), we found that the FK2 ubiquitin antibody did not recognize any ubiquitin signals along autosomes but recognized ubiquitin signals on sex chromosomes (Fig. 6A and B). We observed accumulated FK2 ubiquitin signals along the axes of the sex chromosomes at the early pachytene stage (Fig. 6A, white-dashed circle). At mid to late pachytene, the FK2 ubiquitin signal became more abundant and spread to the entire XY body in *Mamerr*$^{+/+}$ spermatocytes (Fig. 6B, white-dashed circle). In *Mamerr*$^{-/-}$ spermatocytes, however, no ubiquitin signal was detected by the FK2 antibody in the XY body at the early pachytene stage (Fig. 6C, white-dashed circle). In mid to late pachytene *Mamerr*$^{-/-}$ spermatocytes, the ubiquitin signal was completely absent in 75% of the observed cells (Fig. 6D, $n = 20$) and was very low in the remaining 25% of the cells observed (Fig. 6D', $n = 20$). These results indicated that MAMERR promotes ubiquitination of the XY body in pachytene-stage spermatocytes.

2.11. H2A ubiquitination is substantially suppressed in *Mamerr*$^{-/-}$ XY bodies

Chromosomes are made up of structures of nucleosomes, which are composed of a segment of DNA wrapped around eight core histones (H2A, H2B, H3, and H4) in eukaryotes (Kornberg et al., 1974). H2A ubiquitination is highly enriched in XY bodies during the pachytene stage of meiotic prophase I, and this is believed to be associated with gene silencing (Baarends et al., 2005). Thus, we tested whether the dramatic reduction in the ubiquitination of the XY body in *Mamerr*$^{-/-}$ spermatocytes is due to reduced ubiquityl-H2A (Ub-H2A) by using the antibody clone E6C5 that recognizes monoubiquitination of H2A at K119. As shown in Fig. 6E, in *Mamerr*$^{+/+}$ spermatocytes, Ub-H2A signals were present on sex chromosomes at pachytene (Fig. 6E, white-dashed circle). In *Mamerr*$^{-/-}$ spermatocytes, the Ub-H2A signals in the XY body were much lower than in the XY bodies of *Mamerr*$^{+/+}$ spermatocytes (Fig. 6F, white-dashed circle). Thus, the reduced Ub-H2A was likely to be at least partly responsible for the dramatically reduced ubiquitination indicated by the reduced FK2 signal (Fig. 6C and D). It is thus likely that ubiquitination of other proteins is also reduced in the XY body of *Mamerr*$^{-/-}$ spermatocytes. The exact ubiquitin signal densities as measured by the FK2 and E6C5 antibodies were not quantitatively comparable.

2.12. Ubiquitin signals are reduced on autosomes of *Mamerr*$^{-/-}$ spermatocytes

We also tested a rabbit K48-specific ubiquitin antibody clone Apu2-07 that is reported to recognize K-48 ubiquitin chains on autosomes (Rao et al., 2017). K48-linked polyubiquitin chains target proteins for degradation via proteolysis (Hicke, 2001). By immunofluorescence, we found that in control *Mamerr*$^{+/+}$ germ cells, the K48-linked ubiquitin (Ub-K48) signal was located on the autosomal axes at late zygotene (Fig. 6G, arrows) and pachytene (Fig. 6H and H′, arrows) stages, and this was in agreement with previous results (Rao et al., 2017). Ub-K48 antibody–detected ubiquitin signals were also observed on the XY body at the pachytene stage (Fig. 6H, white-dashed circle). Nevertheless, in sharp contrast, the Ub-K48 signal was almost completely absent on autosomes at the late zygotene and pachytene stages (Fig. 6I, J and J') and on XY bodies in *Mamerr*$^{-/-}$ spermatocytes (Fig. 6J, white-dashed circle). These results indicated that the absence of MAMERR in male germ cells not only resulted in substantially reduced ubiquitination of the XY body, but also led to reduced ubiquitination on autosomes. The substantially reduced ubiquitination on autosomes and XY chromosomes is likely an important reason for the observed pachytene arrest and apoptotic cell death in *Mamerr*$^{-/-}$ spermatocytes.

To summarize, the aforementioned data suggested that MAMERR not only regulates ubiquitination of XY bodies that may be of significance in controlling MSCI but also participates in HR and DSB repair by regulating the ubiquitination of autosomes.

2.13. MAMERR is not an E3 ligase or a substrate for ubiquitination

We next studied whether MAMERR *per se* is a possible E3 ubiquitination ligase or is a substrate for ubiquitination. HEK293T cells were cotransfected with *pCMV6-Mamerr-Myc-Flag* and *pCMV-HA-ubiquitin* expression constructs, and the cells were harvested for protein extraction 24 h after transfection. Ectopic MAMERR in whole-cell extract (WCE) was immunoprecipitated using an anti-FLAG antibody, and the eluted proteins were subjected to Western blotting for HA-ubiquitin analysis. In WCE transfected with *HA-*

the pachytene stage are shown (the white-dashed circle indicates the XY body). The enlarged view of the boxed area shows no γH2AX on chromosomes in *Mamerr*$^{+/+}$ spermatocytes (**G′**) and the persistent γH2AX on chromosomes in *Mamerr*$^{-/-}$ spermatocytes (**J′**, yellow arrows). **H** and **K**: Representative images of spermatocytes at the diplotene stage (the white-dashed circle indicates the XY body). **L** and **M**: *Mamerr*$^{+/+}$ and *Mamerr*$^{-/-}$ spermatocytes immunostained for SYCP3 (red) and MLH1 (green, arrows and arrowheads). **N**: *Mamerr*$^{-/-}$ spermatocytes had decreased numbers of MLH1 foci compared with *Mamerr*$^{+/+}$ spermatocytes. Each dot represents the number of MLH1 foci per cell, with black dots indicating *Mamerr*$^{+/+}$ spermatocytes and red dots indicating *Mamerr*$^{-/-}$ spermatocytes. Solid lines show the means and standard deviations of the number of foci in each group of spermatocytes. The *P*-value was calculated using Student's *t*-test. MAMERR, male meiosis recombination regulator; SYCP3, synaptonemal complex protein 3; PD35, postnatal day 35; MLH1, MutL homolog 1.

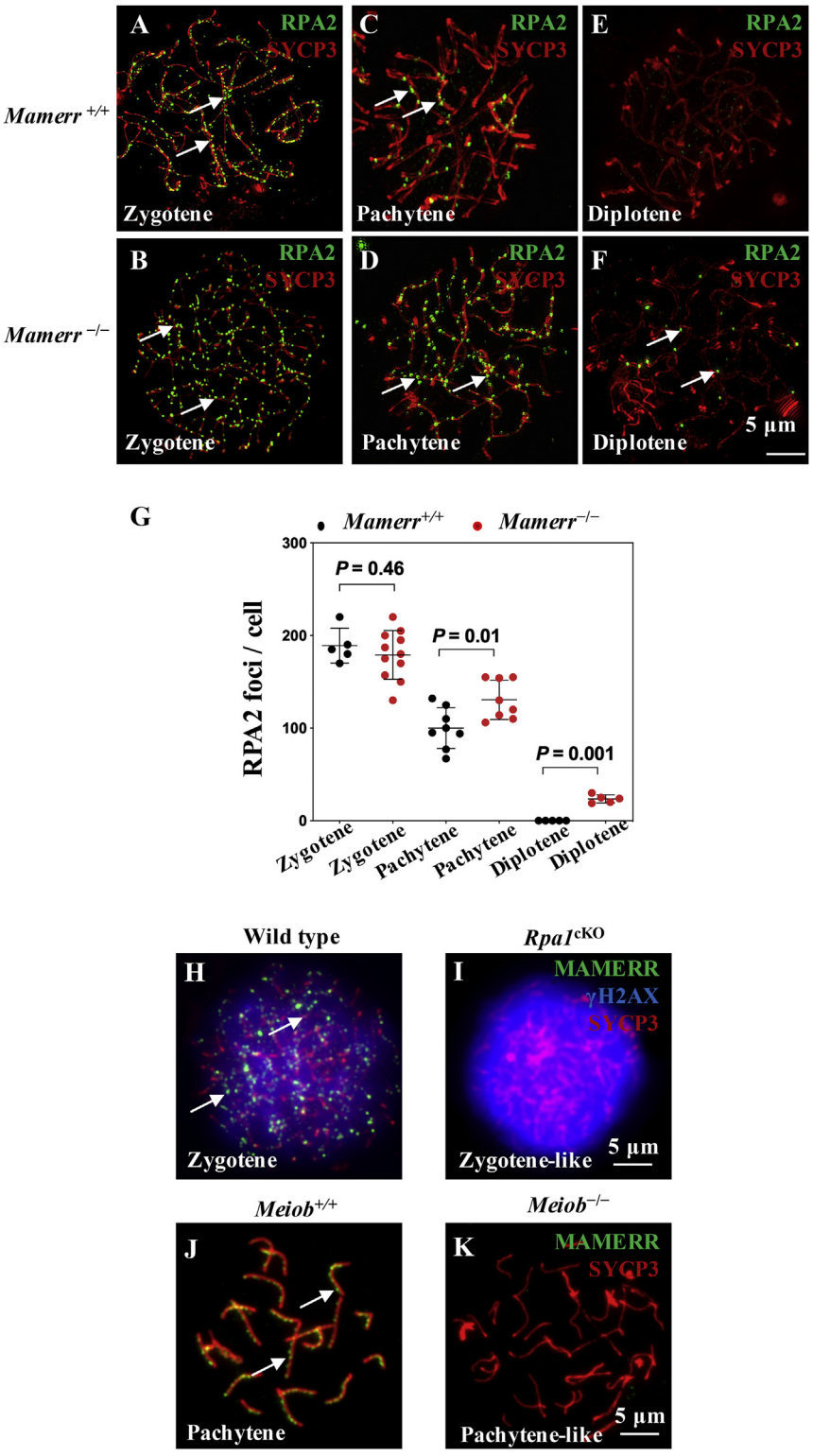

Fig. 4. Localization of MAMERR foci on chromosomes is dependent on RPA and MEIOB/SPATA22 complexes, but not vice versa. **A**–**F**: Immunostaining for SYCP3 (red) and RPA2 (green) in *Mamerr*$^{+/+}$ and *Mamerr*$^{-/-}$ spermatocytes. Representative images of spermatocytes at the zygotene (**A** and **B**), pachytene (**C** and **D**), and diplotene stages (**E** and **F**) are shown. **G**: *Mamerr*$^{-/-}$ spermatocytes had increased numbers of RPA2 foci compared with *Mamerr*$^{+/+}$ spermatocytes at the pachytene and diplotene stages. **H** and **I**: Chromosome spreads of spermatocytes from wild-type and *Rpa1*^{cKO} mice were stained with MAMERR (green, arrows), γH2AX (blue), and SYCP3 (red). There was a strong γH2AX signal and an absence of MAMERR foci in *Rpa1*^{cKO} zygotene-like spermatocytes (**I**). **J** and **K**: Chromosome spreads of spermatocytes from *Meiob*$^{+/+}$ and *Meiob*$^{-/-}$ mice were stained with MAMERR (green, arrows) and SYCP3 (red). There was an absence of MAMERR foci in *Meiob*$^{-/-}$ pachytene-like spermatocytes (**K**). MAMERR, male meiosis recombination regulator; SYCP3, synaptonemal complex protein 3; RPA, replication protein A; MEIOB, meiosis-specific with OB domains; SPATA22, spermatogenesis associated 22.

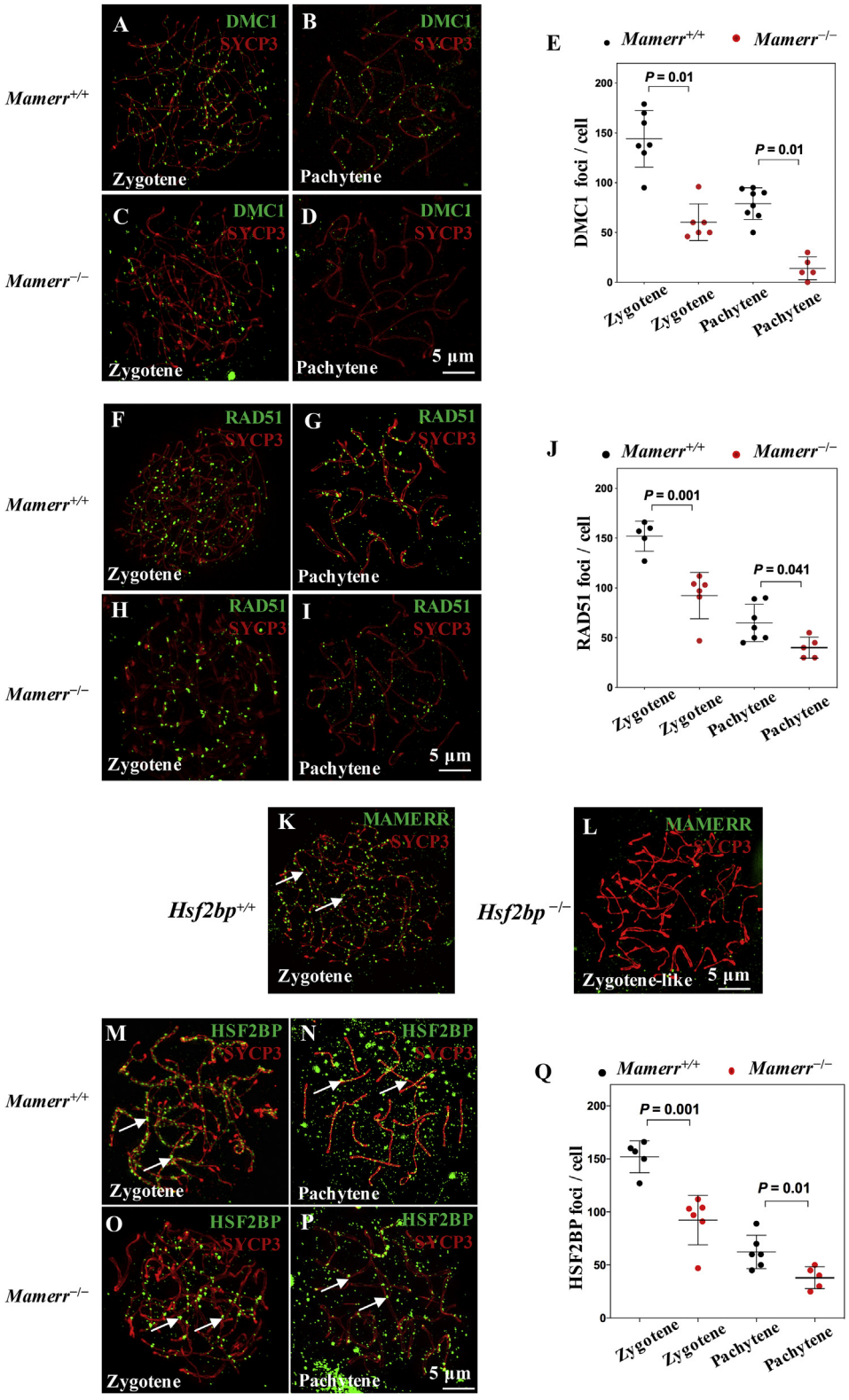

Fig. 5. MAMERR facilitates recruitment of RAD51/DMC1 to DSB sites by regulating HSF2BP localization. **A**–**D**: Immunostaining for SYCP3 (red) and DMC1 (green) in *Mamerr*$^{+/+}$ and *Mamerr*$^{-/-}$ spermatocytes. Representative images of spermatocytes at zygotene (**A** and **C**) and pachytene (**B** and **D**) stages are shown. (**E**) *Mamerr*$^{-/-}$ spermatocytes had decreased numbers of DMC1 foci compared with *Mamerr*$^{+/+}$ spermatocytes from the zygotene to pachytene stages. **F**–**I**: Immunostaining for SYCP3 (red) and RAD51 (green) in *Mamerr*$^{+/+}$ and *Mamerr*$^{-/-}$ spermatocytes. Representative images of spermatocytes at the zygotene (**F** and **H**) and pachytene (**G** and **I**) stages are shown. **J**: *Mamerr*$^{-/-}$ spermatocytes had decreased numbers of RAD51 foci compared with *Mamerr*$^{+/+}$ spermatocytes from the leptotene to pachytene stages. **K** and **L**: SIM images of chromosome spreads of spermatocytes from *Hsf2bp*$^{+/+}$ and *Hsf2bp*$^{-/-}$ mice were stained for MAMERR (green) and SYCP3 (red). MAMERR foci were absent in *Hsf2bp*$^{-/-}$ zygotene-like spermatocytes (**L**). **M**–**P**: Immunostaining for SYCP3 (red) and HSF2BP (green) was performed in *Mamerr*$^{+/+}$ and *Mamerr*$^{-/-}$ spermatocytes. Representative images of spermatocytes at the zygotene (**M** and **O**) and pachytene stages (**N** and **P**) are shown. **Q**: *Mamerr*$^{-/-}$ spermatocytes had decreased numbers of HSF2BP foci compared with *Mamerr*$^{+/+}$ spermatocytes at the zygotene and pachytene stages. Each dot represents the number of indicated protein foci per cell, with black dots indicating *Mamerr*$^{+/+}$ spermatocytes and red dots indicating *Mamerr*$^{-/-}$ spermatocytes. Solid lines show the means and standard deviations of the number of foci in each group of spermatocytes. *P*-values were calculated using Student's t-test. MAMERR, male meiosis recombination regulator; SIM, structured illumination microscopy; SYCP3, synaptonemal complex protein 3; HSF2BP, heat shock factor 2–binding protein; DSB, double-strand break.

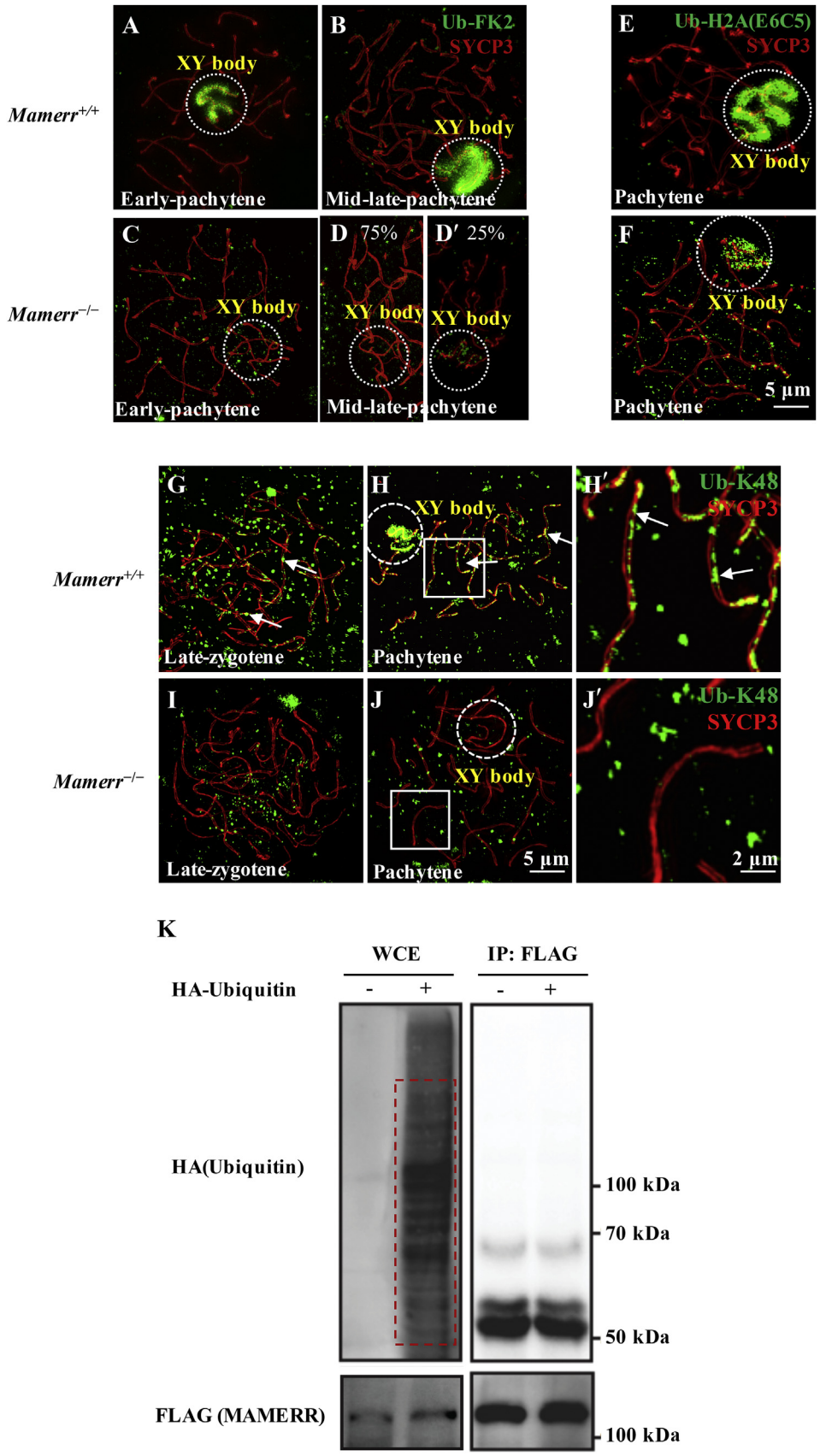

Fig. 6. Ubiquitination of the XY body and autosomes is substantially suppressed in *Mamerr*$^{-/-}$ spermatocytes. **A**–**D**: Immunostaining for SYCP3 (red) and ubiquitin (Clone FK2) (green) was performed in *Mamerr*$^{+/+}$ (**A** and **B**, white-dashed circles indicating the XY body) and *Mamerr*$^{-/-}$ (**C**–**D′**, white-dashed circles indicating the XY body) spermatocytes. Representative images of spermatocytes at the early and mid-late pachytene stages are shown. Early and mid-late pachytene stages were distinguished based on the XY body

ubiquitin, ubiquitinated targets of different molecular weights were detected compared with WCE without HA-ubiquitin (Fig. 6K, red frame). When immunoprecipitating using the anti-FLAG antibody, little HA-tagged ubiquitin was precipitated with the ectopic MAMERR protein (Fig. 6K). In other words, no ubiquitinated species of MAMERR were detected in the *in vivo* ubiquitination assay. Therefore, we conclude that MAMERR is likely not an E3 ligase or a substrate for ubiquitylation.

In summary, we showed that MAMERR is a male-specific meiosis recombination regulator that facilitates meiosis prophase I in males. Deletion of *Mamerr* caused partially disrupted recruitment of the recombination factors HSF2BP and DMC1/RAD51, persistent DSBs, decreased crossover formation, and more noticeably the suppressed ubiquitination of autosomes and XY bodies, thus resulting in pachytene arrest and infertility in males (Fig. 7). It is likely that MAMERR plays some regulatory roles in modifying HSF2BP and other meiotic proteins and thus regulates their recruitments and functions. The mechanisms behind the regulation of meiosis prophase I by MAMERR in male germ cells remain unclear (Fig. 7).

3. Discussion

In recent years, epigenetic factors regulating meiosis prophase I have attracted the attention of researchers (Reynolds et al., 2013; Qiao et al., 2014; Luo et al., 2015; Xu et al., 2016; Rao et al., 2017; Hirota et al., 2018; Li et al., 2019). In this study, we report a new meiosis prophase I–specific gene *Mamerr* that is indispensable for meiosis prophase I and fertility in male mice and that likely regulates meiosis prophase 1 by regulating recombination proteins and by modulating the ubiquitination status on autosomes and XY chromosomes. *Mamerr*$^{-/-}$ spermatocytes suffered from pachytene arrest with substantially reduced ubiquitination on the sex body and autosomes, and this was accompanied by mildly defective DSB repair and partially impaired crossover formation.

Compared with other reported mouse models lacking meiosis prophase I–specific proteins, such as *Rpa1*^{cKO}, *Meiob*-, *Spata22*-, and *Hsf2bp*-deficient mice, the phenotype of *Mamerr*$^{-/-}$ mice is distinct. The *Rpa1*^{cKO}, *Meiob*-, *Spata22*-, and *Hsf2bp*-knockout spermatocytes were all completely arrested at the zygotene stage, with failed synapsis and crossover formation, showing that these proteins may act as indispensable components of the recombination complex for progression to the pachytene stage of meiosis prophase I (La Salle et al., 2012; Luo et al., 2013; Ribeiro et al., 2016; Brandsma et al., 2019). In *Mamerr*$^{-/-}$ spermatocytes, however, chromosome synapsis occurred generally normally, DMC1/RAD51 could be partially recruited, the XY body formed normally, and some recombination sites matured into crossovers. The *Mamerr*$^{-/-}$ spermatocytes were mostly arrested at the pachytene stage, and only 4% of spermatocytes could progress to the diplotene stage. The phenotypes in *Mamerr*$^{-/-}$ spermatocytes seem milder and thus do not support the hypothesis that MAMERR participates in prophase I in a similar fashion as RPA, MEIOB, SPATA22, or HSF2BP. Based on our results that foci of RPA2, SPATA22, HSF2BP, and RAD51/DMC1 were still present at DSBs in *Mamerr*$^{-/-}$ spermatocytes, we propose that MAMERR might play a modifying role, rather than a constructing role, for the recombination-related complex. MAMERR is likely to function as a protein that modifies other proteins, most likely epigenetically, during HR and DSB repair. Our results also raised an interesting point whether *Mamerr* mutations may be a reason for the meiosis arrest in azoospermic men (Enguita-Marruedo et al., 2019).

In *Mamerr*$^{-/-}$ mice, the ubiquitin signal was absent or very low in XY bodies in pachytene spermatocytes, and the role of ubiquitination during meiosis progression represents an extremely important topic (Bose et al., 2014; Rao et al., 2017; Uckelmann and Sixma, 2017). At the pachytene stage, the transcriptionally silenced XY body is marked by accumulated ubiquitin and Ub-H2A signals (Baarends et al., 2005; Lu et al., 2010; Luo et al., 2015; Maezawa et al., 2018). *Ubb*$^{-/-}$ spermatocytes exhibited decreased ubiquitination and were arrested at the pachytene stage (Ryu et al., 2008), and the Ub-H2A signal was found to be decreased in the XY body of *Ubb*$^{-/-}$ spermatocytes; thus, Ub-H2A has been suggested to be essential for maintaining silencing of the asynapsed chromosomes (Ryu et al., 2008; Sinnar et al., 2011). Therefore, the reduced ubiquitination signal in XY bodies of the *Mamerr*$^{-/-}$ spermatocytes seems to be responsible for the pachytene arrest and subsequent cell death.

In addition to the XY body, we also found that the ubiquitination signal was decreased on autosomes at the late zygotene and pachytene stages in *Mamerr*$^{-/-}$ spermatocytes. In a study by Rao et al. (2017), it was reported that the number of RAD51/DMC1 foci during meiosis prophase I was aberrant in spermatocytes treated with a ubiquitin inhibitor, suggesting that ubiquitination regulates the recombination process (Rao et al., 2017). HEI10, which has ubiquitin-ligase activity, was reported to be localized on chromosome axes in a synapsis and recombination-dependent manner (Qiao et al., 2014). The persistent DSB foci on autosomes in *Mamerr*-deficient spermatocytes resemble the phenotype of the *Hei10*-deficient mouse model wherein ubiquitination was repressed on autosomes (Qiao et al., 2014; Rao et al., 2017). The persistence of RPA2 in *Mamerr*$^{-/-}$ spermatocytes at the pachytene stage might be the result of decreased ubiquitination on autosomes because K48-linked polyubiquitin chains function in protein degradation via proteolysis (Hicke, 2001). K48-linked polyubiquitin chains are also involved in transcription regulation, and this might affect the recombination-related protein expression (Oh et al., 2020). Taken together, our results suggest that defective ubiquitination on the autosomes and XY body might be the reason for the pachytene arrest and other related defects in *Mamerr*$^{-/-}$ spermatocytes. Our data showed that MAMERR is likely not an E3 ligase or a substrate for ubiquitylation, and we speculate that MAMERR might function in association with E1 or E2 or, in some other way, to regulate the ubiquitination indirectly.

MAMERR was found to be colocalized with HSF2BP on DSBs, and with *in vitro* biochemical experiments, we showed that MAMERR can be immunoprecipitated with HSF2BP through its 526–575 aa region in cell lines. At this stage, we cannot conclude that in meiosis prophase I, MAMERR binds directly to HSF2BP and facilitates the binding of BRCA2 and further recruits DMC1/RAD51 complexes to DSBs owing to the limited reliability of *in vitro* experimental systems in mammalian cell lines and yeast 2-hybrid systems (Zhang et al., 2020). Because HSF2BP can still localize normally on DSBs

morphology and SYCP3 staining. **E** and **F**: Immunostaining for SYCP3 (red) and Ub-H2A (Clone E6C5) (green) was performed in *Mamerr*$^{+/+}$ (**E**, white-dashed circles indicating the XY body) and *Mamerr*$^{-/-}$ (**F**, white-dashed circles indicating the XY body) pachytene spermatocytes. **G**–**J**: Immunostaining for SYCP3 (red) and Ub-K48 (green) was performed in *Mamerr*$^{+/+}$ (**G** and **H**, arrows, white-dashed circles indicating the XY body) and *Mamerr*$^{-/-}$ spermatocytes (**I** and **J**, white-dashed circles indicating the XY body). Representative images of spermatocytes at the late zygotene and pachytene stages are shown. The enlarged view of the boxed area shows a normal ubiquitination signal on autosomes in *Mamerr*$^{+/+}$ spermatocytes (**H′**, arrows) and decreased signal in *Mamerr*$^{-/-}$ spermatocytes (**J′**). **K**: The *in vivo* ubiquitylation assay showed that no HA-tagged ubiquitin was immunoprecipitated with the MAMERR protein. MAMERR, male meiosis recombination regulator; SYCP3, synaptonemal complex protein 3; Ub-H2A, ubiquityl-H2A; IP, immunoprecipitation; WCE, whole-cell extract.

in the absence of MAMERR, although with decreased efficiency, the possible binding of MAMERR to HSF2BP might not be essential for prophase I progression. Even if MAMERR can pull down HSF2BP in IP experiments with mouse testis lysates, this only means that MAMERR is in the same complex with the recombination proteins. It is most likely that MAMERR plays regulatory roles in modifying the meiotic proteins and thus regulates their functions during DSB repair. Our results suggest that MAMERR is not an E3 ligase or a substrate for ubiquitylation, but MAMERR may function in association with E1 or E2 or in some other way to regulate the ubiquitination on autosomes and XY chromosomes. The regulation of ubiquitination by MAMERR during meiotic prophase I represents a very interesting topic for our future studies. Our results suggest that MAMERR plays a role in DSB repair and HR, which was supported by an independent study with a reliable *Mamerr*-deficient mouse model (Takemoto et al., 2020), but the details of the mechanism behind this remain unclear.

To summarize, our work suggests that the novel meiosis prophase I–specific protein MAMERR regulates the ubiquitination status of autosomes as well as the XY body and thus functions as an indispensable regulator for meiosis prophase I in male mice. We propose that MAMERR might represent a novel epigenetic regulator in male meiosis prophase I.

4. Materials and methods

4.1. Animals

All mice used in this article were in the C57BL/6 genetic background. The *Mamerr*-deficient mouse model was generated in Kui Liu's laboratory by Cyagen Biosciences (Santa Clara, California, USA). The genomic DNA fragment covering exon 3–6 was deleted using the Clustered Regularly Interspaced Short Palindromic Repeats (CRISPR)/CRISPR associated protein 9 (Cas9)-mediated genome editing system. The genotypes of founders were confirmed by PCR and DNA sequencing analysis. The mice were housed under controlled environmental conditions with free access to water and food, and illumination was on between 06:00 and 18:00. All animal breeding and experiments were approved by the Regional Ethics Committee of the University of Hong Kong-Shenzhen Hospital.

Genotyping was performed by PCR amplification of genomic DNA extracted from mouse tails. PCR primers for the *Mamerr* mutant allele were forward: 5′-ACCAGCCTAGCCTTCTTGTTGAA-3′ and reverse: 5′-GTGATGACCCAAGGCTTCCTG-3′, yielding a 599-bp fragment. PCR primers for the *Mamerr* wild-type allele were forward: 5′-TATACACTCTTAACTGCTAGGCTCTC-3′ and reverse: 5′-GTGATGACCCAAGGCTTCCTG -3′, yielding a 301-bp fragment.

The *Hsf2bp*-deficient and *Spo11*-deficient mouse models were ordered from an existing mouse sperm bank of Cyagen Biosciences (Santa Clara, California), which were generated by deleting the genomic DNA fragment covering exons 3–4 and exons 1–13 using the CRISPR/Cas9-mediated genome editing system, respectively.

4.2. Production of the MAMERR antibody

A cDNA fragment encoding amino acids 1–231 of mouse *Mamerr* was cloned into the *pET-32a* (+) vector (Novagene, Beijing, China) and transformed into BL21-CodonPlus (DE3) *Escherichia coli* competent cells. The cells were cultured to an OD_{600} of 0.6 at 37 °C and then induced in the presence of 0.2 μM isopropyl-1-thio-β-D-galactoside (Sigma-Aldrich, Burlington, MA, USA) at 28 °C for 4 h. Bacterial cells were harvested by centrifugation and resuspended in phosphate-buffered saline (PBS). The resuspended cells were sonicated on ice and centrifuged for 30 min at 13,000×*g* at 4 °C. The supernatant was collected and incubated with Ni-NTA Agarose (Qiagen, Shanghai, China) for purification of *Mamerr*. The purification procedure was according to the manufacturer's instructions. The purified protein was dialyzed in PBS and used to immunize rabbits complemented with Complete Freund's Adjuvant or Incomplete Freund's Adjuvant (Sigma-Aldrich, Burlington, MA), and the antiserum of immunized rabbits was affinity purified on antigen-coupled CNBr-activated agarose (GE Healthcare, Chicago, IL, USA).

4.3. Purification of male germ cells

The male germ cells were purified by bovine serum albumin gradient sedimentation (Gan et al., 2013). The seminiferous tubules were cut into several pieces and incubated with 0.2 mg/mL of collagenase (17100017; Gibco, Waltham, MA, USA), 0.25% trypsin (15050057, Gibco, Waltham, MA), and 1 mg/mL of DNase I. The single-cell suspension was filtered through a 40 μm Nylon Cell Strainer (BD Falcon, Franklin Lakes, NJ, USA) and loaded to a cell separation apparatus with a 2–4% bovine serum albumin (BSA) gradient in 600 mL of Dulbecco's Modified Eagle Medium (DMEM). We checked the cell type and purity through the morphological characteristics under a light microscope.

4.4. Tissue collection and histological analysis

Testes from more than three mice for each genotype were dissected, fixed in Bouin's solution (P2210; Solarbio, Beijing, China) for up to 24 h, dehydrated using graded ethanol, embedded, and sectioned. The slides then underwent deparaffinization and were stained with hematoxylin and eosin for histological analysis.

4.5. Immunocytology and antibodies

Spermatocyte and oocyte chromosome spreads were prepared as described previously (Peters et al., 1997; Liu et al., 2019). Primary antibodies used for immunofluorescence were as follows: rat anti-MAMERR (1:100 dilution; homemade), rabbit anti-SYCP3 (1:500 dilution, #ab15093; Abcam, Cambridge, UK), mouse anti-SYCP3 (1:500 dilution, #ab97672; Abcam), rabbit anti-SYCP1(N-terminal) (1:2000 dilution, #A12139; Abclonal, Woburn, MA, USA), rat anti-RPA2 (1:100 dilution, #2208; Cell Signaling Technology, Danvers, MA, USA), rabbit anti-SPATA22 (1:200 dilution; homemade), rabbit anti-HSF2BP (1:200 dilution; homemade), rabbit anti-RAD51 (1:200 dilution, #PA5-27195; Thermofisher Scientific, Waltham, MA, USA), mouse anti-DMC1 (1:100 dilution, # 67176-1-Ig; Proteintech, Wuhan, China), mouse anti-phospho-Histone H2AX ($pSer^{139}$) (1:300 dilution, #05–636; Millipore, Burlington, MA, USA), mouse anti-MLH1 (1:50 dilution, #550838; BD Biosciences, Franklin Lakes, NJ, USA), mouse anti-ubiquitinylated proteins, clone FK2 (1:500 dilution, #04263; Millipore), mouse anti-ubiquityl-histone H2A, clone E6C5 (1:500 dilution, #05678; Millipore), and rabbit anti-ubiquitin antibody, Lys48-specific, clone Apu2-07 (1:100 dilution, #051307; Millipore). Alexa Fluor 488-, 594-, or 647-conjugated secondary antibodies (1:500 dilution, #ab150084, #ab150077, #ab150113, #ab150120, #ab150119, #ab150165, and #ab150168; Abcam) were used to detect the primary antibody. The slides were washed three times with PBS and mounted using VECTASHIELD antifade mounting medium with 4',6-diamidino-2-phenylindole (DAPI) (# H-1200; Vector Laboratories, Burlingame, CA, USA).

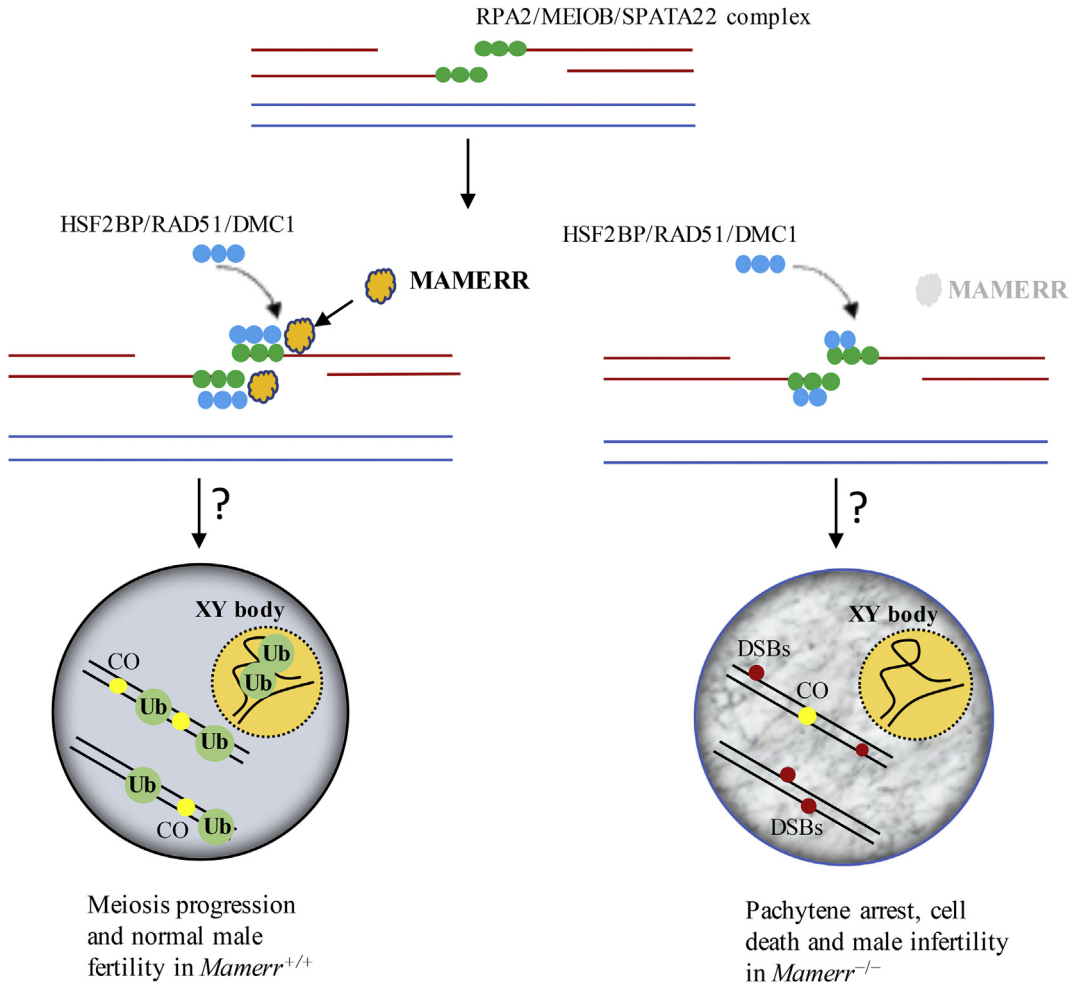

Fig. 7. An illustration of MAMERR regulating meiosis recombination in males. In *Mamerr*$^{+/+}$ spermatocytes, MAMERR colocalized with the RPA and MEIOB/SPATA22 complex. MAMERR regulates ubiquitination on autosomes and XY chromosomes, thus facilitating recruitment of HSF2BP and RAD51/DMC1 proteins, leading to DSB repair and crossover maturation. In *Mamerr*$^{-/-}$ spermatocytes, HSF2BP and RAD51/DMC1 recruitment is mildly decreased accompanied by decreased ubiquitination on autosomes and the XY body. *Mamerr*$^{-/-}$ spermatocytes suffer from persistent DSBs and reduced crossover formation, resulting in pachytene arrest and male infertility. MAMERR, male meiosis recombination regulator; RPA, replication protein A; MEIOB, meiosis-specific with OB domains; SPATA22, spermatogenesis associated 22; HSF2BP, heat shock factor 2–binding protein; DSB, double-strand break.

4.6. RT-PCR

Total RNA was extracted from the testis, ovary, oviduct, uterus, spleen, lung, muscle, thymus, liver and brain of wild-type adult mice and embryonic ovaries. The PrimeScript RT reagent kit with gDNA Eraser (Takara, Shiga, Japan) was used to synthesize cDNA, and PCR was performed using Ex Taq (Takara). *β-actin* was amplified as the internal control. Forward and reverse primers were as follows: *Mamerr* primer pair F 5′-TTC CCT CCC CAT GAC ATC AGA-3′ and R 5′-GCT ACT ACT GTC TTG AAC TGT GG-3′ as well as *β-actin* F 5′-CAT CCG TAA AGA CCT CTA TGC CAA C-3′ and R 5′-ATG GAG CCA CCG ATC CAC A-3′. All RT-PCR reactions were performed as follows: an initial denaturation at 94 °C for 10 min followed by 30 cycles of denaturation at 94 °C for 30 s, annealing at 60 °C for 30 s, and extension at 72 °C for 30 s, and a final extension at 72 °C for 5 min using a T100 Thermal Cycler (Bio-Rad, Hercules, CA, USA).

4.7. Western blotting

Proteins were extracted from testes collected from male C57BL/6 mice using lysis buffer (50 mM Tris-HCl, pH 8.0, 120 mM NaCl, 1 mM ethylenediaminetetraacetic acid (EDTA), 6 mM ethylene glycol-bis(β-aminoethyl ether)-*N*,*N*,*N*′,*N*′-tetraacetic acid (EGTA), 1% NP-40, 1 mM dithiothreitol (DTT), 10 mM NaF, 0.25 mM Na_3VO_4, 50 mM β-glycerolphosphate supplemented with Complete Protease Inhibitor [4693159001; Roche, Switzerland]) (Li et al., 2019). The testes were homogenized thoroughly on ice and then centrifuged at 13,000 rpm for 25 min at 4 °C. The pellet was discarded, and the supernatants were collected for Western blots. Primary antibodies used for Western blotting were rabbit anti-MAMERR antibody (Dia-an Biological Technology Incorporation, Wuhan, China), rabbit anti-GFP antibody (#A11122; Invitrogen, Waltham, MA), rabbit anti-FLAG antibody (#14793S; Cell Signaling Technology), and mouse anti-His antibody (#66005-1-Ig; Proteintech). Secondary antibodies used for Western blotting were horseradish peroxidase–conjugated anti-mouse (dilution, #1721011; Bio-Rad), anti-rabbit (#1706515; Bio-Rad), and anti-rat (#ab6734; Abcam) antibodies. β-actin (#ab227387; Abcam) was used to standardize the loading variations. Antibodies were detected by Clarity Western ECL Substrate (#1705060; Bio-Rad) for film-based imaging.

4.8. IP and antibodies

HEK 293T cells were transiently transfected, with both recombinant plasmids expressing MAMERR and other indicated proteins. The transfected cells were lysed in lysis buffer, and a total of 1 mg of

cell lysate was supplemented with anti-tag antibody or the corresponding IgG as the negative control and incubated for 12 h at 4 °C. The immunocomplexes were isolated using mixed protein A/G Sepharose beads (11719416001 and 11719408001; Roche) for 1 h at 4 °C. After washed five times, the beads were loaded onto 10% sodium dodecyl sulfate–polyacrylamide gel electrophoresis (SDS-PAGE) gels, and the separated proteins were detected by Western blotting with the indicated antibodies. All Western blots were repeated at least three times.

IP analyses were performed using mouse anti-GFP antibody (#66002-1-Ig; Proteintech), mouse anti-FLAG antibody (#66008-3-Ig; Proteintech), mouse anti-His antibody (#66005-1-Ig; Proteintech), mouse IgG (#12–371; Millipore), and rabbit IgG (#12–370; Millipore).

4.9. In vivo ubiquitylation assay

HEK293T cells were cotransfected with 3 μg of *pCMV6-Mamerr-myc-Flag* and 3 μg of *pCMV-HA-ubiquitin* expression constructs. The cells were harvested 24 h after transfection for protein extraction. The collected cells were lysed in 200 μL of NETN buffer (20 mM Tris-HCl [pH 8.0], 100 mM NaCl, 0.5% Nonidet P-40, and 1 mM EDTA) supplemented with benzonuclease (Biotool, Loganholme, Australia) for 5 min on ice, followed by addition of 800 μL of denaturing buffer (20 mM Tris-HCl [pH 8.0], 50 mM NaCl, 0.5% Nonidet P-40, 0.5% deoxycholate, 0.5% SDS, and 1 mM EDTA) and boiling for 10 min. Ectopic MAMERR in these lysates was then immunoprecipitated under denaturing conditions at 4 °C overnight. Beads were washed with denaturing buffer and boiled in SDS sample buffer. The eluted proteins were subjected to Western blotting for analysis.

4.10. Imaging

Immunolabeled chromosome spreads were imaged using a Carl Zeiss LSM 700 inverted confocal microscope driven by Zeiss Efficient Navigation (ZEN) 2011 software (Carl Zeiss, Oberkochen, Germany) for Windows 7 (64-bit). The projection images were then prepared using ZEN 2012 Offline. Histology analysis was performed using an epifluorescence microscope (BX52; Olympus, Tokyo, Japan). Super-resolution images were captured using the Zeiss ELYRA S1 Super Resolution Microscope (Carl Zeiss) driven by Windows 7, ZEN 2.3 and equipped with a 60×/1.42 oil objective, and the images were further processed for structured illumination and maximum projection using Zen 2012 Offline (Carl Zeiss).

4.11. Statistical analysis

All data are presented as mean ± standard deviation. The differences between the mean values from two genotypes were analyzed using Student's *t*-test with a paired, 2-tailed distribution. Statistical significance was set when the *P*-value was less than 0.05.

CRediT authorship contribution statement

Miao Li: Conceptualization, Methodology, Investigation, Writing - original draft, Writing - review & editing, Supervision. **Haiwei Feng:** Methodology, Investigation, Writing - review & editing. **Zexiong Lin:** Methodology, Investigation, Writing - review & editing. **Jiahuan Zheng:** Methodology, Investigation, Writing - review & editing. **Dongteng Liu:** Methodology, Investigation, Writing - review & editing. **Rui Guo:** Methodology. **Junshi Li:** Methodology. **Raymond H.W. Li:** Writing - review & editing, Funding acquisition. **Ernest H.Y. Ng:** Writing - review & editing. **Michael S.Y. Huen:** Writing - review & editing. **P. Jeremy Wang:** Writing - review & editing, Funding acquisition. **William S.B. Yeung:** Writing - review & editing, Funding acquisition. **Kui Liu:** Conceptualization, Writing - review & editing, Funding acquisition, Supervision.

Acknowledgments

This work was supported by grants from the Hong Kong Research Grant Council (17114920, K.L. and R.H.W.L.), the University of Hong Kong (K.L.), the Sanming Project of Medicine in Shenzhen, China (SZSM201612083, W.S.B.Y.), High Level-Hospital Program, Health Commission of Guangdong Province, China (HKUSZH201902018, K.L.), Shenzhen-Hong Kong Innovation Circle Type D (K.L.), and a grant from the NIH/NIGMS (National Institute of General Medical Sciences) R35GM118052 (P.J.W.). We thank Mr. Zhi Li and several other technicians for their kind contributions to this project. We also thank our various colleagues and researchers for constructive discussions.

Supplementary data

Supplementary data to this article can be found online at https://doi.org/10.1016/j.jgg.2020.08.001.

References

Baarends, W.M., Wassenaar, E., van der Laan, R., Hoogerbrugge, J., Sleddens-Linkels, E., Hoeijmakers, J.H., de Boer, P., Grootegoed, J.A., 2005. Silencing of unpaired chromatin and histone H2A ubiquitination in mammalian meiosis. Mol. Cell Biol. 25, 1041–1053.

Baker, S.M., Plug, A.W., Prolla, T.A., Bronner, C.E., Harris, A.C., Yao, X., Christie, D.M., Monell, C., Arnheim, N., Bradley, A., Ashley, T., Liskay, R.M., 1996. Involvement of mouse Mlh1 in DNA mismatch repair and meiotic crossing over. Nat. Genet. 13, 336–342.

Baudat, F., Buard, J., Grey, C., Fledel-Alon, A., Ober, C., Przeworski, M., Coop, G., De Massy, B., 2010. PRDM9 is a major determinant of meiotic recombination hotspots in humans and mice. Science 327, 836–840.

Bose, R., Manku, G., Culty, M., Wing, S.S., 2014. Ubiquitin-proteasome system in spermatogenesis. Adv. Exp. Med. Biol. 759, 181–213.

Brandsma, I., Sato, K., van Rossum-Fikkert, S.E., van Vliet, N., Sleddens, E., Reuter, M., Odijk, H., van den Tempel, N., Dekkers, D.H.W., Bezstarosti, K., Demmers, J.A.A., Maas, A., Lebbink, J., Wyman, C., Essers, J., van Gent, D.C., Baarends, W.M., Knipscheer, P., Kanaar, R., Zelensky, A.N., 2019. HSF2BP interacts with a conserved domain of BRCA2 and is required for mouse spermatogenesis. Cell Rep. 27, 3790–3798 e3797.

Cloud, V., Chan, Y.L., Grubb, J., Budke, B., Bishop, D.K., 2012. Rad51 is an accessory factor for Dmc1-mediated joint molecule formation during meiosis. Science 337, 1222–1225.

Edelmann, W., Cohen, P.E., Kane, M., Lau, K., Morrow, B., Bennett, S., Umar, A., Kunkel, T., Cattoretti, G., Chaganti, R., Pollard, J.W., Kolodner, R.D., Kucherlapati, R., 1996. Meiotic pachytene arrest in MLH1-deficient mice. Cell 85, 1125–1134.

Enguita-Marruedo, A., Sleddens-Linkels, E., Ooms, M., de Geus, V., Wilke, M., Blom, E., Dohle, G.R., Looijenga, L.H.J., van Cappellen, W., Baart, E.B., Baarends, W.M., 2019. Meiotic arrest occurs most frequently at metaphase and is often incomplete in azoospermic men. Fertil. Steril. 112, 1059–1070 e1053.

Gan, H., Wen, L., Liao, S., Lin, X., Ma, T., Liu, J., Song, C.X., Wang, M., He, C., Han, C., Tang, F., 2013. Dynamics of 5-hydroxymethylcytosine during mouse spermatogenesis. Nat. Commun. 4, 1995.

Handel, M.A., Schimenti, J.C., 2010. Genetics of mammalian meiosis: regulation, dynamics and impact on fertility. Nat. Rev. Genet. 11, 124–136.

Hasegawa, K., Sin, H.S., Maezawa, S., Broering, T.J., Kartashov, A.V., Alavattam, K.G., Ichijima, Y., Zhang, F., Bacon, W.C., Greis, K.D., Andreassen, P.R., Barski, A., Namekawa, S.H., 2015. SCML2 establishes the male germline epigenome through regulation of histone H2A ubiquitination. Dev. Cell 32, 574–588.

Hays, E., Majchrzak, N., Daniel, V., Ferguson, Z., Brown, S., Hathorne, K., La Salle, S., 2017. Spermatogenesis associated 22 is required for DNA repair and synapsis of homologous chromosomes in mouse germ cells. Andrology 5, 299–312.

Hicke, L., 2001. Protein regulation by monoubiquitin. Nat. Rev. Mol. Cell Biol. 2, 195–201.

Hirota, T., Blakeley, P., Sangrithi, M.N., Mahadevaiah, S.K., Encheva, V., Snijders, A.P., Ellnati, E., Ojarikre, O.A., de Rooij, D.G., Niakan, K.K., Turner, J.M.A., 2018. SETDB1 links the meiotic DNA damage response to sex chromosome silencing in mice. Dev. Cell 47, 645–659.e6.

Ichijima, Y., Ichijima, M., Lou, Z., Nussenzweig, A., Camerini-Otero, R.D., Chen, J., Andreassen, P.R., Namekawa, S.H., 2011. MDC1 directs chromosome-wide silencing of the sex chromosomes in male germ cells. Genes Dev. 25, 959–971.

Jensen, R.B., Carreira, A., Kowalczykowski, S.C., 2010. Purified human BRCA2 stimulates RAD51-mediated recombination. Nature 467, 678–683.
Keeney, S., Neale, M.J., 2006. Initiation of meiotic recombination by formation of DNA double-strand breaks: mechanism and regulation. Biochem. Soc. Trans. 34, 523–525.
Kornberg, R.D., 1974. Chromatin structure: a repeating unit of histones and DNA. Science 184, 868–871.
La Salle, S., Palmer, K., O'Brien, M., Schimenti, J.C., Eppig, J., Handel, M.A., 2012. *Spata22*, a novel vertebrate-specific gene, is required for meiotic progress in mouse germ cells. Biol. Reprod. 86, 45.
Li, M., Huang, T., Li, M.J., Zhang, C.X., Yu, X.C., Yin, Y.Y., Liu, C., Wang, X., Feng, H.W., Zhang, T., Liu, M.F., Han, C.S., Lu, G., Li, W., Ma, J.L., Chen, Z.J., Liu, H.B., Liu, K., 2019. The histone modification reader ZCWPW1 is required for meiosis prophase I in male but not in female mice. Sci. Adv. 5, eaax1101.
Liu, H., Huang, T., Li, M., Li, M., Zhang, C., Jiang, J., Yu, X., Yin, Y., Zhang, F., Lu, G., Luo, M.C., Zhang, L.R., Li, J., Liu, K., Chen, Z.J., 2019. SCRE serves as a unique synaptonemal complex fastener and is essential for progression of meiosis prophase I in mice. Nucleic Acids Res. 47, 5670–5683.
Lu, L.Y., Wu, J., Ye, L., Gavrilina, G.B., Saunders, T.L., Yu, X., 2010. RNF8-dependent histone modifications regulate nucleosome removal during spermatogenesis. Dev. Cell 18, 371–384.
Lu, L.Y., Xiong, Y., Kuang, H., Korakavi, G., Yu, X., 2013. Regulation of the DNA damage response on male meiotic sex chromosomes. Nat. Commun. 4, 2105.
Luo, M., Yang, F., Leu, N.A., Landaiche, J., Handel, M.A., Benavente, R., La Salle, S., Wang, P.J., 2013. MEIOB exhibits single-stranded DNA-binding and exonuclease activities and is essential for meiotic recombination. Nat. Commun. 4, 2788.
Luo, M., Zhou, J., Leu, N.A., Abreu, C.M., Wang, J., Anguera, M.C., de Rooij, D.G., Jasin, M., Wang, P.J., 2015. Polycomb protein SCML2 associates with USP7 and counteracts histone H2A ubiquitination in the XY chromatin during male meiosis. PLoS Genet. 11, e1004954.
Maezawa, S., Hasegawa, K., Alavattam, K.G., Funakoshi, M., Sato, T., Barski, A., Namekawa, S.H., 2018. SCML2 promotes heterochromatin organization in late spermatogenesis. J. Cell Sci. 131, jcs217125.
Oh, E., Mark, K.G., Mocciaro, A., Watson, E.R., Prabu, J.R., Cha, D.D., Kampmann, M., Gamarra, N., Zhou, C.Y., Rape, M., 2020. Gene expression and cell identity controlled by anaphase-promoting complex. Nature 579, 136–140.
Peters, A.H., Plug, A.W., van Vugt, M.J., de Boer, P., 1997. A drying-down technique for the spreading of mammalian meiocytes from the male and female germline. Chromosome Res. 5, 66–68.
Qiao, H., Prasada Rao, H.B., Yang, Y., Fong, J.H., Cloutier, J.M., Deacon, D.C., Nagel, K.E., Swartz, R.K., Strong, E., Holloway, J.K., Cohen, P.E., Schimenti, J., Ward, J., Hunter, N., 2014. Antagonistic roles of ubiquitin ligase HEI10 and SUMO ligase RNF212 regulate meiotic recombination. Nat. Genet. 46, 194–199.
Rao, H.B., Qiao, H., Bhatt, S.K., Bailey, L.R., Tran, H.D., Bourne, S.L., Qiu, W., Deshpande, A., Sharma, A.N., Beebout, C.J., Pezza, R.J., Hunter, N., 2017. A SUMO-ubiquitin relay recruits proteasomes to chromosome axes to regulate meiotic recombination. Science 355, 403–407.
Reynolds, A., Qiao, H., Yang, Y., Chen, J.K., Jackson, N., Biswas, K., Holloway, J.K., Baudat, F., de Massy, B., Wang, J., Hoog, C., Cohen, P.E., Hunter, N., 2013. RNF212 is a dosage-sensitive regulator of crossing-over during mammalian meiosis. Nat. Genet. 45, 269–278.
Ribeiro, J., Abby, E., Livera, G., Martini, E., 2016. RPA homologs and ssDNA processing during meiotic recombination. Chromosoma 125, 265–276.
Ryu, K.Y., Sinnar, S.A., Reinholdt, L.G., Vaccari, S., Hall, S., Garcia, M.A., Zaitseva, T.S., Bouley, D.M., Boekelheide, K., Handel, M.A., Conti, M., Kopito, R.R., 2008. The mouse polyubiquitin gene *Ubb* is essential for meiotic progression. Mol. Cell Biol. 28, 1136–1146.
Shi, B., Xue, J., Yin, H., Guo, R., Luo, M., Ye, L., Shi, Q., Huang, X., Liu, M., Sha, J., Wang, P.J., 2019. Dual functions for the ssDNA-binding protein RPA in meiotic recombination. PLoS Genet. 15, e1007952.
Sinnar, S.A., Small, C.L., Evanoff, R.M., Reinholdt, L.G., Griswold, M.D., Kopito, R.R., Ryu, K.Y., 2011. Altered testicular gene expression patterns in mice lacking the polyubiquitin gene *Ubb*. Mol. Reprod. Dev. 78, 415–425.
Soh, Y.Q., Junker, J.P., Gill, M.E., Mueller, J.L., van Oudenaarden, A., Page, D.C., 2015. A gene regulatory program for meiotic prophase in the fetal ovary. PLoS Genet. 11, e1005531.
Takemoto, K., Tani, N., Takada-Horisawa, Y., Fujimura, S., Tanno, N., Yamane, M., Okamura, K., Sugimoto, M., Araki, K., Ishiguro, K.I., 2020. Meiosis-specific C19orf57/4930432K21Rik/BRME1 modulates localization of RAD51 and DMC1 to DSBs in mouse meiotic recombination. Cell Rep. 31, 107686.
Thorslund, T., Esashi, F., West, S.C., 2007. Interactions between human BRCA2 protein and the meiosis-specific recombinase DMC1. EMBO J. 26, 2915–2922.
Turner, J.M., 2007. Meiotic sex chromosome inactivation. Development 134, 1823–1831.
Uckelmann, M., Sixma, T.K., 2017. Histone ubiquitination in the DNA damage response. DNA Repair 56, 92–101.
Wold, M.S., 1997. Replication protein A: a heterotrimeric, single-stranded DNA-binding protein required for eukaryotic DNA metabolism. Annu. Rev. Biochem. 66, 61–92.
Xu, Y., Greenberg, R.A., Schonbrunn, E., Wang, P.J., 2017. Meiosis-specific proteins MEIOB and SPATA22 cooperatively associate with the single-stranded DNA-binding replication protein A complex and DNA double-strand breaks. Biol. Reprod. 96, 1096–1104.
Xu, Z., Song, Z., Li, G., Tu, H., Liu, W., Liu, Y., Wang, P., Wang, Y., Cui, X., Liu, C., Shang, Y., de Rooij, D.G., Gao, F., Li, W., 2016. H2B ubiquitination regulates meiotic recombination by promoting chromatin relaxation. Nucleic Acids Res. 44, 9681–9697.
Zhang, J., Gurusaran, M., Fujiwara, Y., Zhang, K., Echbarthi, M., Vorontsov, E., Guo, R., Pendlebury, D.F., Alam, I., Livera, G., Emmanuelle, M., Wang, P.J., Nandakumar, J., Davies, O.R., Shibuya, H., 2020. The BRCA2-MEILB2-BRME1 complex governs meiotic recombination and impairs the mitotic BRCA2-RAD51 function in cancer cells. Nat. Commun. 11, 2055.
Zickler, D., Kleckner, N., 1999. Meiotic chromosomes: integrating structure and function. Annu. Rev. Genet. 33, 603–754.
Zickler, D., Kleckner, N., 2015. Recombination, pairing, and synapsis of homologs during meiosis. Cold Spring Harb. Perspect. Biol. 7, a016626.